Co/Ni(111) superlattices studied by microscopy, X-ray absorption and *ab-initio* calculations

M. Gottwald [1,3], S. Andrieu[1*], F. Gimbert[2], E. Shipton [3], L. Calmels[2], C. Magen[4,5], E. Snoeck[2,5], M. Liberati [6], T. Hauet [1], E. Arenholz [6], S. Mangin [1], E. Fullerton [3]

[1]*Institut Jean Lamour, UMR 7198 Nancy University - CNRS, 54506 Vandoeuvre France*

[2]*CEMES-CNRS, UPR 8011 , Université de Toulouse, 29 rue Jeanne Marvig, 31055 Toulouse, France*

[3]*Center for Magnetic Recording Research, University of California, San Diego, La Jolla, CA 92093-0401USA*

[4] *Laboratorio de Microscopías Avanzadas (LMA), Instituto de Nanociencia de Aragón (INA)-ARAID, Universidad de Zaragoza, 50018 Zaragoza, Spain*

[5]*Transpyrenean Associated Laboratory for Electron Microscopy, CEMES – INA, CNRS – University of Saragossa*

[6]*ALS, Berkeley USA*

* corresponding author

Abstract

We explore the origins of perpendicular magnetic anisotropy in epitaxial and textured Co/Ni (111) superlattices using a combination of thin film growth, structural characterization, x-ray magnetic circular dichroism (XMCD) and *ab-initio* calculations. Transmission electron microscopy and x-ray diffraction experiments allow us to show that the "bulk" magnetoelastic contribution to the total magnetic energy is small compared to the interface anisotropy. The magnetic properties are studied by using XMCD at the Co and Ni $L_{2,3}$ edges. Hysteresis loops performed at the Co L_3 edge confirm the perpendicular magnetization for Co thicknesses up to 4 monolayers. The spin and orbital moments were deduced using the XMCD sum rules. The results are explained by considering two kinds of magnetic moments for Co, distinguishing the interfaces from the rest of the layers. Both effective spin and orbital moments of Co atoms are found to be enhanced at the Co-Ni interfaces, whereas the magnetic moment of Co surrounded by Co is similar to the bulk values. *Ab-initio* calculations allow us to show a strong enhancement of the dipole operator contribution on Co atoms at the interface that is partly responsible for this high effective spin moment at the interface. Such a moment enhancement is not observed for Ni, the dipole operator contribution being close to zero. Finally, we observed a very surprising proportionality between the effective spin and orbital moments, independent of the absorption edge or deposition technique used. We assign this peculiar behavior to the fact that the magnetic dipole operator involved in the sum rules is closely linked to the increase of the Co orbital moment at the interface. Based on XMCD results obtained on both molecular beam epitaxy and sputter deposited samples, this link allows us to show the extreme sensitivity of the perpendicular anisotropy with the chemical ordering at the interface.

Introduction

[Co/Ni] superlattices (SLs) have been extensively studied over the last 20 years driven by their unusual magnetic properties; they exhibit perpendicular magnetic anisotropy (PMA) and unusual transport and magneto-transport characteristic. Co and Ni are closely lattice matched ($a_{Co,fcc}$= 0.35447 nm [1] and $a_{Ni,fcc}$= 0.35236 nm [2]) resulting in growth of high-quality superlattices where the strain in each layer is well estimated from coherent growth models [3]. Despite the fact that Co and Ni are both magnetic transition metals, PMA was predicted and experimentally demonstrated for [Co(1ML)/Ni(2 ML)] fcc (111) superlattices in 1991 by Daalderop et al. [4]. This has resulted in extensive experimental and theoretical studies of the origin of PMA in this system. The initial calculations [4] suggest that the PMA arises from a combination between a Néel type Co-Ni interface anisotropy and the interface electronic structure. They show that the electronic structure for [Co(1ML)/Ni (2ML)] superlattices close to the Fermi energy consists of bands with $(x^2\text{-}y^2)$ and xy character, what favors perpendicular anisotropy. Kyuno et al. [5] found similar results confirming the role of a large local density of states of $|m_l|$= 2 character for the PMA of Co/Ni multilayers.

In experimental studies strong evidence for Co/Ni interfacial PMA was found. Several authors [6-11] studied PMA as a function of the Co layer thickness and report a maximum of PMA for Co thicknesses between 1 and 2 monolayers (MLs), which is consistent with an interface anisotropy model. Co/Ni perpendicular interface anisotropy was not only shown for (111), but also for (100) and (110) oriented superlattices [6,7]. However, the strongest interface anisotropy can be found in the case of (111) oriented samples. In addition, the magneto-crystalline contribution for the (111) structures also contributes to PMA, which leads to a relatively broad range of Co and Ni thicknesses with out of plane magnetization in the case of (111)-oriented superlattices. Tuning of growth conditions, substrates, and seed layers was reported to be essential in order to increase the (111) texture and hence the PMA of Co/Ni multilayers [12-15]. For applications also post-deposition techniques like annealing [16] and ion irradiation [17] were studied as tools to tailor the magnetism of Co/Ni superlattices. In the case of annealing the perpendicular anisotropy can be enhanced due to an improvement of the crystalline structure, whereas PMA can be decreased by ion irradiation due to intermixing of the Co/Ni interface.

Further interest in [Co/Ni] superlattices has been driven by their unusual transport properties. First, unusual high anisotropic magnetoresistance (AMR) values could be obtained [18-24] and attributed to the Co/Ni interfaces [25]. Second Gallego et al. [26-28] reported an oscillatory behavior of the electrical resistance of [Co/Ni] superlattices as a function of the layer periodicity. Those oscillations were explained by electron localization in the superlattice structure and motivated band structure calculations [29-31]. However, predicted effects of localized electrons, which are thought to

be responsible for the resistance oscillations, on the elastic properties of [Co/Ni] superlattices could not be confirmed [32].

Renewed interest into [Co/Ni] superlattices arose from the discovery of spin transfer torque effects [33-35] in magnetic nanopillars. First experimental demonstrations of spin transfer torque reversal of magnetization were done in systems with magnetic in-plane anisotropy [36]. High current densities (10^8 A/cm^2) were needed to switch magnetization, as the created torque has to overcome the demagnetizing field in this geometry. This additional increase of the necessary current densities could have been avoided by using materials with out of plane anisotropy. However typical materials with PMA like $L1_0$ phase alloys, rare-earth –transition-metal alloys or multilayers containing Pt or Pd tend to have high Gilbert damping parameter α and mostly low spin polarization P, what strongly decreases the spin transfer torque efficiency for these materials. The reason for their high Gilbert damping parameters α and low spin polarizations P compared to 3d metals is the fact that these materials contain high Z-elements which give rise to strong spin-orbit coupling. [Co/Ni] superlattices have PMA and they only contain 3d transition metals. Experimentally low switching currents for perpendicular magnetized nanopillars consisting of spin valves based on [Co/Ni] superlattices compared to similar [Co/Pt] based samples could be demonstrated [37]. Furthermore, high efficiency for current induced domain wall motion in [Co/Ni]-based nanowires could also be demonstrated [38]. As a consequence of their high spin transfer torque efficiency and their tunable magnetization and anisotropy [4-17], [Co/Ni] superlattices became a model system for spin transfer torque studies in PMA systems. First of all it could be shown that by tuning the anisotropy of [Co/Ni] for nanopillars with spin valve structure, the critical currents for spin torque could be further reduced, while thermal stability was maintained, what is a key point towards applications [39,40]. Another studied effect was the creation of domain walls in nanostructures driven by spin-polarized currents [41] and concomitant telegraph noise [42]. [Co/Ni] based samples were also used by several authors to explore the dynamics of magnetic moments under spin transfer torque: [Co/Ni] superlattices were used as free layer in spin torque driven oscillators [43,44], the relations between current pulse length, pulse intensity and thermal activation for spin torque induced magnetization reversal [45] and ultrafast switching of magnetic moments under spin torque were analyzed [46]. Moreover, insight could be given on the influence of microwaves on spin torque driven magnetization precession [47] and the use of magnetic susceptibility measurements as a probe of spin transfer driven magnetization dynamics [48]. In addition distortions of the Stoner-Wohlfarth astroid by spin-polarized currents were observed [49] in nanopillars with [Co/Ni] free layer. Finally the influence of the pillar geometry on spin transfer torque switching was studied [50]. As mentioned above, the high efficiency of spin transfer torque in nanopillars based on perpendicular [Co/Ni] spin valve structures, is due to a small α/P value for [Co/Ni] superlattices. Investigations have though been carried out to get better insight in spin polarization and Gilbert damping and to further enhance these properties for the [Co/Ni] system.

Gilbert damping in [Co/Ni] superlattices was measured using vector network analyser ferromagnetic resonance [51], spin-torque-driven ferromagnetic resonance [52] and by time-resolved magneto-optical Kerr measurements [53] and found to be of the order of 0.03-0.04. Ion irradiation of [Co/Ni] multilayers was shown to only reduce PMA but not the intrinsic Gilbert damping parameter [54]. Further investigations showed that α seems to be independent from anisotropy fields [55] but can be tuned by varying the relative Co and Ni content of the multilayer [56]. Apart for the damping, a large polarization is also needed to get low critical current. GMR values for [Co/Ni] based spin valves of up to 8% [57] indicate a strong potential of this material to spin polarize electric currents. An optimization of the spin polarization by increasing the number of Co/Ni bilayers in a superlattice was discussed but found to be useless due to an important spin flip rate at the Co/Ni interface [58]. First principle calculations show a spin polarization of up to 70% at the Fermi level [59] which is significantly higher than the 42 % for Co, but this point has to be confirmed by experiments.

The Co/Ni system was also used in other directions. Using [Co/Ni] nanowires, important contributions to the understanding of the role of pinning in current driven domain wall (DW) motion [60] could be made using the spin torque effect. Furthermore non-adiabatic [61] and adiabatic [62] spin torques could be measured, what allowed to progress in the comprehension of current induced domain wall motion. It should be pointed out that the good understanding of DW propagation in Co/Ni-based nanowires lead to the development of logic and memory devices for technological applications [63,64]. Beside its convenience as a model system for spin torque experiments, [Co/Ni] multilayers were also used to increase PMA of CoFeB layers in magnetic tunnel junctions [65,66] and to enhance the switching properties of bit patterned media [67,68]. For both applications again the tunable magnetization and PMA were a key point.

Although those macroscopic magnetic properties of the Co/Ni system have now been confirmed extensively, several important questions still remain. First, this PMA was attributed to a Néel type interface anisotropy in addition to the bulk crystalline anisotropy (easy axis along 111). Another contribution may also come from magneto-elastic anisotropy which can be large in this particular system, but this point was not clearly addressed. Second, the atomic magnetic properties are still unclear. An increase of the Co spin moments and a decrease of Ni spin moments measured by XAS and XMCD experiments [69,70] as well as no significant change of the magnetic moments at the interface were reported [71]. Recent *ab-initio* calculations find a small increase of the spin moments at the Co/Ni interface [72]. Moreover, the thicknesses range to get PMA is very different for sputtered *vs.* epitaxial films, and the reason is not yet clear. The aim of this work is first to evaluate the magneto-elastic contribution by looking at the strain in the system, and second to bring insight into the determination of atomic moments in Co/Ni(111) superlattices, using detailed XMCD measurements compared with *ab-initio* calculations.

2 – MBE grown Co/Ni(111) layers

Sample preparation

A first series of samples were prepared by using molecular beam epitaxy (MBE). The Co/Ni(111) layers are deposited on a seed layer constituted of first V(110) and second Au(111) seed layers grown on sapphire substrates. The Co and Ni thicknesses were accurately controlled by using reflection high energy electron diffraction (RHEED). By recording the intensity of the RHEED truncation rods during the growth, we observed intensity oscillations (called RHEED oscillations) during the growth of Ni on the Au(111) buffer layer, and during the growth of Co on Ni. This means that Ni (Co) grows layer by layer on Au (Ni). The period of the oscillations is exactly the time to complete an atomic plane, and takes around 40 sec for Ni and 80 sec for Co in our experimental conditions. Such low growth rates allow us to control the deposition time and consequently the thicknesses with accuracy lower than 0.1ML. The Co/Ni layers are deposited at room temperature and no thermal intermixing is observed. More details about the growth are given in [10]. Two kinds of samples were prepared by MBE. First, $(Co_x/Ni_y)xN$ superlattices were grown varying x from 0.1 to 4 ML, y from 1 to 4 ML, and keeping N=5. Second, two wedges were prepared with the architecture Ni (3ML) / Co (xML) / Ni (3ML) with x = 0.25, 0.5, 0.75, 1, 1.5, 2 MLs for the first wedge and x = 2, 3, 4, 5, 7, 10 MLs for the second one. All samples were capped by MgO to prevent any oxidation on air. MgO was also chosen because of its low x-Ray absorption behavior compared to Au for instance.

Origin of PMA: magnetostriction vs. interface ?

To understand the relative contributions of magnetostriction vs. interface anisotropy we studied the superlattices by both Cu K_{α} x-ray diffraction (XRD) and scanning transmission electron microsopy (STEM). The STEM studies were performed on a FEI Titan 60-300 kV microscope fitted with a probe aberration corrector (CEOS) allowing forming a probe size below 0.1 nm. As the contrast between Ni and Co being weak using electrons, Co and Ni layers cannot be distinguished using normal TEM viewing. However, chemical analyses can be carried on cross sectional samples by high-angle-annular-dark-field (HAADF) imaging. In this mode, an annular detector collects the electrons which are incoherently scattered at high angles, whose intensity increases with the average atomic number (Z) of the atomic columns. Thus, aberration corrected STEM-HAADF allows obtaining atomic resolution Z-contrast images, which is not achievable in conventional HRTEM mode due to lack of strong chemical contrast [73]. In addition, quantitative measurements of the strain state of the stacking were performed using the geometrical phase analyse (GPA) method [74]. The top panel of Figure 1 shows a large field of view HAADF STEM image of the whole superlattice stacking. The gold layers which have the highest atomic number (Z_{Au} = 79) appear the brightest, whereas darker areas correspond to the Co/Ni stacks. Optimizing the contrasts within the Co/Ni stacking regions, a

weak contrast modulation is observed that can be attributed to the small Z difference (Z_{Co} = 27, Z_{Ni} = 28) between the alternating Co and Ni layers (Figure 1 insets). These results confirm the layer by layer 2D-growth of the bilayers and the absence of any clear Co and Ni intermixing. The measurements of the bilayer period in the two Co/Ni stacks indicate a period of 1.2 nm for the upper one and 1.0 nm for the lower one, in good agreement with the nominal thickness of the Co/Ni bilayers. Atomic resolution HAADF images can also be obtained thanks to the probe corrector. Figure 1 (bottom left) displays the crystal structure of the Co/Ni stack of the spin valve sample observed along the <110> zone axis. The FCC structure of the Co/Ni layer is evidenced over the entire multilayer with the A-B-C stacking of the (111) planes. This clearly demonstrates the coherent growth of the Co-Ni multilayer. The cobalt (nickel) atomic planes continue the stacking layer of nickel (cobalt) on which they are deposited. This is observed in the Co thickness range from 1 to 3ML. For thick Co layers, the stacking should change to ABAB but we have not addressed this point here. Finally, we have used GPA to analyze the deformation state of the Co/Ni stacking. The measurement of the deformation of the (111) stacking of the Co/Ni in the growth direction relative to the (111) planes of the Au layer is reported in Figure 1 (bottom right). The (111) Au interplanar distance is found to be about 15% larger than the Co/Ni one. The lattice mismatch between FCC Ni (Co) and Au is of that magnitude, thus confirming the totally relaxed growth of Au on Ni/Co and vice versa. It should be noted that this Au incommensurate growth process on Co/Ni is also observed by RHEED (sensitive only to the top surface for grazing incidence electron beam). Indeed, an incommensurate growth between Au and Co/Ni should lead to two different lattices on RHEED patterns during the growth of the first Au atomic plane. Since the misfit is large, we actually observed double streaks corresponding to both Au and Co/Ni surface lattices. Meanwhile, no variation is observed within the Co/Ni stacking (within the spatial resolution of the GPA method used here). This is consistent with the similar (111) lattice spacing of bulk FCC Ni and Co lattice spacing - respectively equal to 0.2034 nm and 0.2046 nm, and with the (111) spacing observed in HAADF images of ~0.20 nm.

This STEM analysis thus clearly indicates that Co and Ni layers are pseudomorphic and constrain coherently with each other, but they are not constrained by Au. This important conclusion has a great impact to evaluate the magnetoelastic energy in these films. The general magnetoelastic energy per volume e_{magel} may be written as [75]:

$$e_{magel} = \left(B_{bulk} + \frac{B_s}{d}\right)\varepsilon \tag{1}$$

where d is the thickness of the layer, B_{bulk} and B_s the bulk and surface magnetoelastic coefficients, and ϵ the strain in the sample. We thus need to know the strain in the film, which can be calculated using this mutual Co and Ni pseudomorphic growth by minimizing the total elastic energy [76]. First, the in-plane lattice resulting from mutual stress between Co and Ni at equilibrium is calculated. Second the out-of-plane lattice spacing in Co and Ni are thus calculated using the elastic relationship

6

between stress and strain. Furthermore, these calculations may be tested by measuring both the in-plane and out-of-plane lattice spacing in the superlattice by using X-Ray Diffraction (XRD). Finally, by using the bulk magnetoelastic coefficient of Co and Ni, the bulk part of the total magnetoelastic energy may be evaluated.

In such an elastic approach, the in-plane lattice spacing $a_{//}$ is constant throughout the structure and is fixed by the minimization of the total elastic energy density stored in the superlattice (e_{elast} energy per unit volume). If we assume first that both Ni and Co structures are isotropic on the elastic point of view (that is if we consider that $C_{11}-C_{12}=C_{44}$), the total elastic energy can be expressed as [77]:

$$e_{elast} = \frac{1}{2}\Sigma_{i \neq j}\sigma_{ij}\varepsilon_{ij} = \left\{\left(A\epsilon_{//}^2\right)_{Co} + \left(A\epsilon_{//}^2\right)_{Ni}\right\} \text{ with } A = \left(\frac{1-\nu}{E}\right)n \text{ and } \varepsilon_{//} = \frac{a_{//}-a_0}{a_0} \quad (2)$$

where E is the Young's modulus, ν the Poisson's ratio, n the thicknesses of the Co and Ni layers and a_0 the lattice parameter of the relaxed structures. The minimization of this energy density leads to the value of the in-plane lattice distance as:

$$a_{//} = a_{Ni}(1-\alpha) + a_{Co}\alpha \qquad \text{with} \qquad \alpha = \frac{A_{Co}}{A_{Ni}+A_{Co}} \quad (3)$$

Knowing the in-plane lattice distance, we can calculate the out-of-plane distance in each Co and Ni layers, and finally the out-of-plane lattice spacing for the superlattice <d>, defined as the average of lattice distances in each Ni and Co layer weighted by the respective number of atomic planes, as [76]:

$$< d >= \frac{n_{Co}d_{Co}+n_{Ni}d_{Ni}}{n_{Co}+n_{Ni}} \quad (4)$$

where n_{Co} and n_{Ni} are the number of monolayers that are accurately known with the help of RHEED oscillations, and d_{Co} and d_{Ni} the (111) lattice spacing in each layers. Such a model may be tested by XRD measurements. In Fig.2 the XRD spectra (using Cu Kα anode) obtained on a (Co3ML/Ni3ML) x75 superlattice are reported. A first measurement was performed with the scattering wavevector perpendicular to the stacking in order to get the (111) peak of the superlattice, and consequently <d> in the previous equation. A second experiment was performed with the scattering wavevector in the plane of the stacking, allowing us to determine the in-plane lattice (220) distance, noted $a_{//}$ below. Finally in Table1 the experimental and calculated values for this model are reported, using the bulk fcc Ni and Co lattice spacing respectively equal to 0.35236 nm and 0.35447nm [2]. We also include calculations in the general non-isotropic case [78]. The agreement between experiment and calculation is excellent, confirming the mutual constraint layers of Co and Ni apart from Au. Furthermore, the mutual strain between Co and Ni is very small since the misfit is only 0.6%. It should be noted that this direct measurement of the strain in this system is in very good agreement with the results deduced from nuclear magnetic resonance reported in [79]. In the case of our cubic structures where the

magnetization is along (111), the "bulk" part of the magnetoelastic energy is thus estimated for a bilayer by using the bulk magnetoelastic coefficient of Co and Ni as [75]:

$$E_{magel}(bulk) = \left\{B_2(\varepsilon_{//} - \varepsilon_\perp)\right\}_{Ni} + \left\{B_2(\varepsilon_{//} - \varepsilon_\perp)\right\}_{Co} \tag{5}$$

where $B_2^{Co} = -29 \, MJ/m^3$ and $B_2^{Ni} = +10 \, MJ/m^3$. The different stress values are given for the sample measured by XRD in Table 1. We thus obtained a magnetoelastic energy for one bilayer of +0.2 MJ/m³. It should be noted that this energy is positive, which means that it contributes to the PMA. This value has to be compared to the total magnetocrystalline + interface anisotropy found in our earlier work, which is $K_V + 2K_s/d \cong +5 MJ/m^3$ for one monolayer of Co [10,11]. This finally leads to an important conclusion: the strong perpendicular anisotropy observed in this system cannot be explained by taking into account only the "bulk" magnetoelastic contribution, in contrast with the Ni/Cu(001) system for instance [80].

This conclusion suggests that rather than the strain the quality of the interface may play an important role to get a large PMA. To test this assumption, a SL was grown by inserting a given amount of Ni atoms in the last atomic plane of Co. This can be made easily by opening the Ni cell shutter just before closing the Co cell shutter with a delay that can be adjusted to get the proper Co to Ni ratio. We performed such an experiment by inserting 10% Ni atoms in the last Co atomic planes in contact with Ni layers. The anisotropy is thus examined by measuring the corresponding hysteresis loop and comparing it with the hysteresis loop obtained on a regular sample with no intermixing. We clearly observe a strong decrease of the PMA. The interfacial origin of the PMA is again confirmed and the chemical quality of the interface is thus a crucial ingredient to get large PMA in this system.

XAS results

The X-Ray Magnetic Circular Dichroism measurements were performed at the Advanced Light Source on beamline B04. Absorption measurements with linear polarization were first performed on the two wedges. In Fig. 3b the XAS measurement at the Co and Ni *L3* edges are shown. The variation of the Co and Ni edges as a function of the thickness of Co is shown in Fig.3c-d. It should be noted that the magnitude of the Ni edge slightly decreases for increasing Co thickness which results from the increased absorption of the upper Co layer with increased thickness. Moreover, we notice a discrepancy between the Ni edge intensity variations with the Co thickness for one wedge compared to the other. This discrepancy comes from the thickness of the MgO capping layer slightly different for the two wedges (about half an atomic plane) and is easy to correct.

These Ni and Co edges intensity variations may be modeling by considering that the total yield *I* can be expressed as a sum of the contribution of the nth atomic plane attenuated by the n-1 planes on top of it so :

$$I = \sum_n I_1(n)K^n \qquad \text{with} \quad K = exp - \frac{1}{\lambda} \qquad\qquad (6)$$

where K is the attenuation factor for one atomic plane which is linked to the escape depth λ, and $I_1(n)$ the monolayer contribution from the nth atomic plane. This $I_1(n)$ is usually considered as constant but here we have to be careful. Indeed, the edge intensities of transition metals in XAS are proportional to the number of holes in the d-bands [83]. In our superlattices, it is absolutely not obvious that this number of holes is the same for each atomic plane in the stacking. However, these numbers of holes variations with Co and Ni thicknesses were calculated using *ab-initio* calculations and are very small, so we may consider that $I_1(n)$ are roughly constant with n. We can thus plot the edge variation as a function of Co thickness, and determine the electrons escaping depth, using the equation:

$$I_{Co} = K_{MgO+Ni} I_{Co}^\infty (1 - K_{Co}^n) \qquad\qquad (7)$$

where n is the number of Co atomic planes, K_{MgO+Ni} is the attenuation factor through the MgO capping layer and Ni layer on top of Co, and K_{Co} the attenuation factor of a Co atomic plane. We get $\lambda = 12 \pm 0.5\ ML$ (Fig.3), in agreement with published values [81,82]. Finally, it is also possible to plot the Co to Ni edge intensity ratio which is of great interest since it is independent of the thickness of the capping. The Ni intensity is calculated using the same method used for getting eq.(7). For our wedges stacking this ratio is finally equal to:

$$\frac{I_{Co}}{I_{Ni}} = \frac{I_{Co}^\infty}{I_{Ni}^\infty} \left\{ \frac{K_{Ni}^2 (1 - K_{Co}^n)}{(1 - K_{Ni}^2) + K_{Ni}^2 K_{Co}^n (1 - K_{Ni}^3)} \right\} \qquad \text{and} \qquad K_{Co} \cong K_{Ni} = e^{\frac{-1}{\lambda}} \qquad\qquad (8)$$

where I_{Co}^∞ and I_{Co}^∞ are the total yield corresponding to thick Co and Ni layers. As the Co and Ni edges are close in energy, the mean free paths are theoretically very close, which has been shown experimentally by Nakajima *et al.* [81]. Thus the only parameter which is not known in eq.(8) is the $I_{Co}^\infty / I_{Ni}^\infty$ ratio. This ratio is equal to the ratio of number of holes in Co and Ni. To get them, we performed XMCD measurements on thick epitaxial hcp Co(0001) and fcc Ni(111) films, applied the sum rules to get the spin and orbital moments per holes, and compared them to their magnetizations measured using macroscopic magnetic measurements (SQUID and VSM). We get $n_h^{Co} = 2.55 \pm 0.1$ and $n_h^{Ni} = 1.1 \pm 0.1$, giving $I_{Co}^\infty / I_{Ni}^\infty \cong 2.3 \pm 0.3$ The edge intensity ratio in eq.(8) can thus be calculated without adjustable parameters, and compared to measurements. The agreement between experiment and calculation is excellent as shown in Fig. 3f. All these results confirm the sample quality and give an experimental determination of the Co to Ni number of holes ratio.

XMCD results

The XMCD measurements were performed at the Co and Ni $L_{2,3}$ edges using nearly 100% polarized circular light applying the field perpendicular to the film plane. The orbital and magnetic

moments were determined by applying the sum rules proposed by Thole *et al.* and Carra *et al.* [84,85] and using the procedure proposed in Ref.86. The field was varied in the range 0-0.5 T. The measurements were performed in total yield for both left and right circular polarization and magnetic field in both directions along the normal of the surface, leading to 4 absorption curves σ^{ij} (i = +,- light polarization , and j = +,- magnetic field direction). Such measurements allow us to eliminate the asymmetry by calculating the absorption curves using $\sigma^+ = \sigma^{++} + \sigma^{--}$ and $\sigma^- = \sigma^{+-} + \sigma^{-+}$. The XMCD spectrum is thus given by $\sigma^+ - \sigma^-$ and the integral of and the isotropic edge used to obtain the integral r is here defined as $(\sigma^+ + \sigma^-)/2$. The orbital momentum sum rule is thus given by:

$$m_{orb} = \langle L_z \rangle \frac{\mu_B}{\hbar} = n_h \cdot \left(\frac{2q}{3r}\right) \mu_B \qquad (9)$$

The PMA is linked to the anisotropy of the orbital moment from in-plane to out-of-plane [83]. Such information is possible to obtain by performing XMCD measurements applying the magnetic field in-plane and out-of-plane [83]. However, magnetic fields larger than 1T are necessary to align the magnetization in-plane in these samples. As the maximum field that can be applied is limited to 0.5T, it was not possible to get the in plane orbital moment in our samples.

The spin sum rule gives the *effective* spin angular momentum which depends on the actual spin angular momentum, on n_h the number of holes in the *d*-bands for the atom under consideration, and on $< T_z >$ the z-component of the spin magnetic dipole operator and is given by :

$$m_{spin}^{eff} = 2\langle S_z^{eff} \rangle \frac{\mu_B}{\hbar} = 2\langle S_z \rangle \frac{\mu_B}{\hbar} \left(1 + \frac{7}{2} \frac{\langle T_z \rangle}{\langle S_z \rangle}\right) = n_h \cdot \left(\frac{3p-2q}{r}\right) \mu_B \qquad (10)$$

where *p* and *q* correspond to the dichroic spectrum, respectively integrated over the *L₃* and over the *L₃+L₂* edges, respectively. *r* is the area of the isotropic *L₂,₃* edge which has to be measured in order to determine the absolute value of the effective spin and orbital magnetic moments. n$_h$ is not known and is very difficult to obtain with a sufficiently good accuracy in experiments. The spin magnetic dipole operator is expressed as:

$$\boldsymbol{T} = \sum_i \boldsymbol{s}_i - 3\frac{\boldsymbol{r}_i(\boldsymbol{r}_i.\boldsymbol{s}_i)}{r_i^2} \qquad (11)$$

where $\boldsymbol{s}_i$ and $\boldsymbol{r}_i$ are the spin angular momentum and position vector of the ith electron. The spin magnetic dipole operator provides detailed information on the anisotropy of the electron spin-density distribution distorted by the crystal field and the spin-orbit coupling [87] and the average z-component $< T_z >$ can be calculated by first principles methods for *3d* metals. The contribution of $< T_z >$ to m_{spin}^{eff} is usually neglected when analyzing the XMCD spectra of bulk *3d* magnetic metals (the electron spin-density is rather isotropic in this case). However, this contribution should not be neglected for magnetic materials containing interfaces [88]. We are typically in such a situation where

10

$< T_z >$ can have a significant contribution to m_{spin}^{eff} for Co and Ni atoms at the interfaces. We use the procedure proposed in Ref.86 to determine *p, q,* and *r*. For very thin Co thicknesses a baseline has to be subtracted to determine *r*. The uncertainty on the magnetic moments values is thus larger for very thin Co or Ni films since it depends on the choice of the baseline.

For the two wedged samples, the hysteresis loops were first measured at the Co L_3 edge for each Co thickness by applying the field perpendicular to the layers in the range -0.05 to 0.05 T (Fig.4). The magnetization is observed perpendicular to the layer plane from 0.25ML to 4ML of Co, with a coercive field increasing for Co thicknesses up to around 1.5ML and then decreasing for larger Co thicknesses. These results confirm those obtained previously [10,11].

The atomic moments were deduced from the sum rules on XMCD measurements performed on the wedges and on a series of superlattices. An example is reported in Fig.5, showing the determination of *p* and *q* without any adjustment of the spectra. It should be noted that the asymmetries are eliminated since the difference between the absorption curves is zero between the edges. This means that the XMCD signal is obtained using raw absorption data, and is afterward integrated without any data correction. The ratio of Co and Ni orbital moments, which only depends on *p* and *q* area needed to calculate the magnetic moments, is thus not data treatment dependent. The variation of (9p-6q) versus 2q is also plotted in Fig.5 for Co and Ni edges and for MBE and sputtered samples (detailed in the next section). Surprisingly, we find a linear variation passing through the origin (as it should be since 2q=0 and 9p-6q=0 for a non-magnetic material), showing that the ratio of the *effective* spin moment on the orbital moment is constant for Co and Ni and is independent on the Co thickness, and on the growth technique used.

The dependence of the orbital and effective spin magnetic moments are plotted *vs.* Co thickness. The results on Co are shown in Fig.6. We notice that for small Co thicknesses the orbital moment reaches 0.21 ± 0.02 μ_B/at. This is an increase of approximately 20% compared to the bulk value, we determined to be 0.16 ± 0.02 μ_B/at. In parallel, we also observe an increase of the effective spin moment. This result is not surprising since we found that the ratio of these two quantities is constant. At this stage it is instructive to plot the magnetic moments according to the inverse of the thickness (Fig.6 right panel). Two regimes are then clearly observed. In a first regime between 0 and 2 ML the Co moments are constant, and a linear regime occurs beyond 2 ML. This result leads us to assume that the Co moments are not the same for atoms located at the interface. In superlattices, Co atoms are sometimes surrounded by only Co atoms (for thick Co layers), and sometimes by both Co and Ni atoms (at the interfaces). Indeed, if we simplify the situation by considering only two contributions, m_1 the Co moment at the Co/Ni interface and m_2 the "bulk" Co moments for Co atoms between 2 Co layers, the average atomic moment can be written as (t_{Co} is the Co layer thickness):

For $\quad 0 \leq t_{Co} \leq 2ML \qquad < m >= m_1$ (12a)

For $\quad 2ML \leq t_{Co} \qquad < m >= \frac{2m_1 + (t_{Co}-2)m_2}{t_{Co}} = \frac{2(m_1 - m_2)}{t_{Co}} + m_2$ (12b)

Two linear regimes are actually obtained depending on the inverse of the Co thickness. Applying this model to the experimental results of Fig.6, this allows us to determine for Co:

$$m_1^{spin-eff} = 2.0 \pm 0.1\mu_B \qquad \text{and} \qquad m_1^{orb} = 0.21 \pm 0.02\mu_B$$ (13a)

$$m_2^{spin-eff} = 1.50 \pm 0.1\mu_B \qquad \text{and} \qquad m_2^{orb} = 0.165 \pm 0.02\mu_B$$ (13b)

A strong increase of the effective spin and orbital Co moments are thus observed at the interface. Moreover, the bulk values are found for the Co atoms just below the interfacial atomic plane.

The Ni moments are shown in Fig. 7. It should be noted here that only the superlattices are analyzed. Indeed, the Ni moments obtained on the two wedge samples are smaller. This is understood by noting that the top Ni layer is in contact with the capping MgO layer where hybridization with MgO decreases the Ni moment. We do not have this problem in the superlattices which were capped with gold. In the SLs, the Ni effective spin moment is observed to slightly increase when Co thickness increases, but this variation is small compared to error bars and is not related to those observed on Co. The Ni orbital moment is also observed to be quite constant when varying the Co thickness and is similar to the bulk one. Finally, measurements on superlattices with a constant Co thickness (1 ML) but with a variable thickness of Ni (1, 2, 3 and 4 ML) show that the moments of Co and Ni do not vary with the thickness of Ni.

All these results allow us to conclude that at the Co/Ni interface, the Co effective spin and orbital moments increase whereas these moments are quite constant for Ni. The increase of the Co orbital moment perpendicular to the plane at the Co/Ni interface is around 20% compared to its bulk value, and may explain the strong interface anisotropy of this system. However, the situation is not as clear concerning the effective spin moments. The strong enhancements of these effective spin moments at the interface do not mean that the true spin moments follow the same variation. Indeed, this increase can be due to a strong increase of the $< T_z >$ contribution at the interfaces. This point is likely as we do not observe a large increase in the average saturation magnetization M_S for thin Co layers that would be expected for a large increase in $< S_z >$. This point is examined via *ab-initio* calculation in latter section.

3 –Co/Ni (111) sputtered samples

To compare with the MBE samples a series of samples were prepared by DC magnetron sputtering with a base pressure of 5x10^{-9} Torr. The samples were deposited on Si (100) substrates at room temperature. Sputtering rates were calibrated using X-ray reflectivity measurements. Grown film compositions were Ta(30Å) / Pd(30Å) / [Co(y)/Ni(6Å)]x10 / Co(3Å) / Pd(7Å)/Ta(10Å) where y =0-4.5 Å. The XMCD experiments on these sputtered samples are the same than those performed on MBE samples (same runs). The same process is used to get the effective spin and orbital moments using the sum rules. The results are shown in Fig. 8. The Co effective spin moments are also observed to be larger than the bulk but are slightly smaller than in the MBE samples. This is the same for the orbital moments, and again the Co orbital moment is observed to increase at the Co/Ni interface. The Ni moments are also observed to be smaller but the difference with MBE samples is not as high as for Co. Both Ni orbital and effective spin moments seem not to change comparing with the bulk. Thus the lower PMA observed in sputtered samples compared to MBE ones may come from these differences between Co orbital and spin moments rather than Ni moments. Indeed, the PMA is observed up to 4-ML Co in MBE samples, as it disappears above 2-ML in the sputtered samples. But another very important result is shown in Fig. 5, together with the results obtained on MBE samples: the ratio of the effective spin to orbital moments is very similar to those obtained in MBE samples. What could explain that MBE and sputtered samples seem to have a very similar moments ratio whereas effective spin and orbital moments are smaller on sputtered samples than on MBE ones? We will see in the following that this could be explained by the fact that the effective spin moment depends on the dipole operator that varies in the same way as the orbital moment.

4 – First-principle calculations of the spin and orbital magnetic moments

The electronic and magnetic structure of the Co$_{xML}$/Ni$_{3ML}$ superlattices has been calculated using the first principles code Wien2k [89] within the local spin density approximation (LSDA). We considered *fcc* superlattices with lattice parameters given by the Vegard law $(3a_{Ni} + x.a_{Co})/(3+x)$, using the lattice constants $a_{Ni} = 0.352$ nm and $a_{Co} = 0.355$ nm of bulk *fcc* Ni and Co. We have checked that the relaxation of the atom coordinates in the unit cell of these superlattices is negligible (the forces acting on the atoms are very small) and does not significantly change the spin and orbital magnetic moments. We used atomic spheres with a radius of 0.124 nm for all the atoms. For 3*d* transition metals, the agreement between the magnetic moments calculated with codes based on the density functional theory (DFT) and measured experimentally is in general better for the spin than for the orbital magnetic moments [90]. This can be seen from the calculated magnetic moments of bulk

fcc Ni and hcp Co described in Tables 2 and 3. The orbital moments are indeed usually underestimated by DFT-based codes, which do not always allow recovering the orbital configuration predicted by the second empirical Hund's rule [91]. Eriksson *et al*. [90] have proposed to add an orbital polarization correction which mimics the second Hund's rule. This correction has given values of the orbital magnetic moments in agreement with experiments for bulk $3d$ transition metals [90]. The improvement due to the polarization correction is however less satisfactory for magnetic atoms at interfaces [92]. The orbital polarization correction has been implemented in the code Wien2k [93].

The spatial variations of the calculated spin magnetic moments are similar in the cobalt and nickel layers, with a small enhancement for the interface monolayers followed by small oscillations as described in Table 4. The values calculated for bulk *fcc* Co (and *fcc* Ni) are recovered at the center of the Co (Ni) layers providing that these layers are thick enough. In the following, we will only discuss Co_{xML}/Ni_{3ML} superlattices with cobalt thicknesses between 1 and 5 MLs. In this case, the spin magnetic moment is respectively 2% and 3% higher at the cobalt and nickel interface layers than in the corresponding *fcc* bulk metals. These non-trivial spatial variations of the spin magnetic moments are responsible for small oscillations of the averaged Co spin magnetic moment $< m_{spin} >$ as a function of the Co layer thickness, see Fig. 9. The Co thickness dependence of $< m_{spin} >$ differs from the variations of $\langle m_{spin}^{eff} \rangle$ measured by XMCD analysis: the strong enhancement observed for $\langle m_{spin}^{eff} \rangle$ as the cobalt layer thickness decreases is not observed for $< m_{spin} >$. The discrepancy between these two averaged spin magnetic moments is actually due to the contribution of the spin magnetic dipole operator. We calculated $< T_z >$, the value of the spin magnetic dipole for different atoms in the superlattices [94-96]. The results are given in Table 5. We have also calculated the value of the spin magnetic dipole averaged over the different Co and Ni atoms of the superlattices. These averaged values are represented in Fig. 10 as a function of the Co layer thickness. It is not negligible for Co atoms and increases strongly for thin Co layers. The results are different for Ni atoms for which $< T_z >$ can be neglected. These differences between Co and Ni atoms can be understood from the spatial variations of the spin magnetic dipole shown in Table 5 and in the inset of Fig. 10 for Co_{5ML}/Ni_{3ML}: For Co atoms, $< T_z >$ increases strongly at the interface layers and slightly oscillates in the other atomic layers. By contrast, positive *and* negative oscillations are strong in the Ni layers, resulting in a negligible contribution of $< T_z >$ in $\langle m_{spin}^{eff} \rangle$. The enhancement of $\langle m_{spin}^{eff} \rangle$ which was measured experimentally for thin Co layer thicknesses is also obtained in the calculated results when the contribution of $\langle T_z \rangle$ is taken into account, as shown in Fig. 9. For Ni atoms, $\langle m_{spin}^{eff} \rangle \approx \langle m_{spin} \rangle$ and the calculated value does not strongly depend on the Co layer thickness.

The orbital magnetic moment shows small spatial oscillations in the Co layers, with maximum values at the interfaces, minimum values in the center of the Co layers, and oscillation amplitudes of

only about 4% of the value calculated for fcc bulk Co (0.124 μ_B when the orbital polarization correction is included, see Table 6). Consequently, the averaged value of the Co orbital magnetic moment $\langle m_{orb} \rangle$ does not strongly depend on the Co layer thickness and takes values between 0.123 and 0.126 μ_B. For Ni atoms, the orbital magnetic moments are smaller at the interfaces than in the central atomic layer, except for Co(1 ML)/Ni(3 ML). The averaged $\langle m_{orb} \rangle$ varies with the Co thickness between 0.061 and 0.065 μ_B (these values are smaller than the 0.069 μ_B calculated for bulk *fcc* Ni).

The small discrepancy which appears between the calculated and experimental values of $\langle m_{orb} \rangle$ and $\langle m_{spin}^{eff} \rangle$ (even when the effects of $\langle T_z \rangle$ are taken into account) could be attributed to the fact that the same number of holes in the *d*-bands has been used for all the superlattices (2.55 holes for Co and 1.1 hole for Ni), while these numbers actually change from one superlattice to the other. The values of n_h are difficult to obtain with a sufficient accuracy according to our experiment and are difficult to calculate from first principles. n_h would be easy to calculate for an isolated atom, but not for a crystal because of the hybridization between the atomic orbitals of the different atoms. Let's assume that n_h could be obtained, for each atom, from the energy integral of the corresponding partial density of *d*-states (*d*-DOS). A difficulty appears because we don't know the energy range in which the *d*-DOS should be integrated: the upper energy from which the electron states do not belong to the *d*-bands is not obvious. Moreover, the valence electron density does not vanish in the interstitial area between atomic spheres: this interstitial charge should also be taken into account. In order to get some information on the variations of n_h with the Co layer thickness, we have integrated the *d*-DOS for Ni and cobalt atoms to roughly estimate the changes in the number of *d*-electrons per atom, from one superlattice to the other. We have compared the averaged integrated *d*-DOS calculated for the superlattices with those calculated for *hcp* Co: this comparison shows that the number of minority spin *d*-electrons for Co atoms would decrease approximately by 0.08 electrons in Co(1 ML)/Ni(3 ML) and by less than 0.02 electrons in all the other superlattices. Similar comparison has been done for Ni atoms, which shows that the number of minority spin *d*-electrons would decrease by approximately 0.1 electrons in Co(1 ML)/Ni(3 ML) and by less than 0.05 electrons in the other systems. This analysis finally shows that the variations of the number of holes are very small both for Ni and Co. The assumption that the numbers of holes are constant when applying the sum rules is thus justified.

5 – Discussion

The growth of epitaxial Co/Ni SLs on Au is not pseudomorphic, leading to a quite small strain in the SLs. The determination of this strain allows us to calculate the bulk magnetoelastic energy, which is shown to be much lower than the contribution of the bulk and interface magnetocrystalline energies. However, *it should be noted that a magnetoelastic contribution coming from the interfaces*

15

cannot be excluded. Indeed, it has been shown that such a contribution may be very large, several tens time the bulk contribution. However, since this interface magnetoelastic term has the same energy expression as the interface anisotropy (K/d), it is difficult to disentangle the two as clearly pointed out in Ref. 75. It is highly possible that both effects play a role. Nevertheless, this definitely demonstrates that the origin of the PMA has to be assigned to the interfaces where this interface anisotropy is large, nearly four times larger than the magnetocrystalline anisotropy of bulk *hcp* Co.

The analysis of the Co and Ni absorption edges (XAS) using a linear polarization is also very instructive. First, our experiments performed on the wedges allow us to extract the electron escape depth in this system. We found 12 ± 0.5 ML in very good agreement with previous measurements [81-83,86]. But the other very important result deals with the number of holes. *Ab-initio* calculations give 2.5 holes for bulk Co and 1.5 holes for bulk Ni [83, 88]. Our XMCD results are consistent with a number of holes close to 2.55 for Co and 1.1 for Ni, which is confirmed in another way by fitting exactly the XAS result without any parameter adjustment. This analysis finally shows that the number of holes calculated and reported in the literature is consistent with the experimental value for Co, but not for Ni atoms. This is not the first time that such a problem is highlighted for Ni [69, 70, 83, 88], but we show here that the Ni number of holes that should be taken into account in XAS and XMCD should be close to 1.1 rather than 1.5. The discrepancy with the calculated value is not yet understood.

More details about magnetic properties at the atomic scale are obtained from the XMCD analysis. We first discuss the effective spin moments obtained using the spin sum rule. The effective spin moment of Co atoms is observed to strongly increase at the interfaces, on the contrary to Ni for which this moment is the same at the interfaces or in the inner Ni atomic layers. These results are explained by *ab-initio* calculations. The calculated magnetic dipole operator contribution in the sum rule is observed to be strong for Co atoms at the interface, whereas its average contribution is close to zero for Ni. The increase of the effective spin moment of Co is consequently an artifact and the calculations show that the true magnetic moments are close to the bulk ones. We observe a clear increase of the orbital moment contribution along (111) for Co atoms at the interface with Ni, both in MBE and sputtered samples. It should be noted that this increase is similar to what has been observed in the Co/Au system [97]. For Ni a slight increase of the perpendicular orbital moment seems to occur when increasing the Co thickness but the error bars are too large to definitely conclude. If this increase is real, it cannot be associated to the interface but rather to the quantity of Co and may be related to magnetoelastic effects in the Ni. Indeed, this increase is observed for a fixed Ni thickness when increasing the Co thickness, whereas no effect was observed when varying the Ni thickness for a fixed Co thickness. Our results indicate that the interfacial anisotropy responsible for the large PMA in Co/Ni is correlated with an increase of the Co perpendicular orbital moment at the interface.

For all our studies we observe a surprising linear variation between the orbital and effective spin moments whatever the absorption edge and the growth technique used. We can explain this observation in the case of Co by using the same approach as for the XMCD analysis: we consider that the magnetic moments result from two contributions, one from Co in contact with Ni at the interfaces, and the other from the Co layer not in contact with Ni that is designed as a bulk contribution. The effective spin and orbital moments can thus be written as the sum of a contribution from the bulk plus a contribution from the interfaces as (t_{Co} being the Co thickness in ML) :

$$< S_z >_{eff} = < S_z >_{eff}^{bulk} + \eta \Delta S_z \qquad \text{and} \qquad < L_z > = < L_z >_{bulk} + \eta \Delta L_z \qquad (14a)$$

with $\begin{cases} t_{Co} \leq 2ML \rightarrow \eta = 1 \\ t_{Co} \geq 2ML \rightarrow \eta = \frac{2}{t_{Co}} \end{cases}$ and $\begin{cases} \Delta S_z = < S_z >_{eff}^{interface} - < S_z >_{eff}^{bulk} \\ < S_z >_{eff}^{interface} = < S_z >_{interface} + \frac{7}{2} < T_z > \\ \Delta L_z = < L_z >_{interface} - < L_z >_{bulk} \end{cases}$ (14b)

According to the *ab initio* calculation we know first that the $< T_z >$ contribution in the bulk of Co layers is close to zero so $< S_z >_{eff}^{bulk} \cong < S_z >_{bulk}$. With this hypothesis, we can thus write ΔS_z as:

$$\Delta S_z = < S_z >_{interface} - < S_z >_{bulk} + \frac{7}{2} < T_z > = \Delta S_{z\, interface} + \frac{7}{2} < T_z > \qquad (14c)$$

Consequently, the increase of the effective spin moment at the interface may come from a combination of a possible increase of the true spin moment at the interface and the effect of $< T_z >$. According to *ab initio* calculations, there is actually an increase of the spin moment at the interface but it is rather small (around 3%, see table 3). However, we will see after that our experiments suggest a larger increase. We can thus write the equation for the ratio of the effective spin and the orbital magnetic moments as a function of the corresponding bulk values as follows:

$$\frac{2<S_z>_{eff}}{<L_z>} = \frac{2<S_z>}{<L_z>}\bigg|_{bulk} \cdot \left(\frac{1+\eta a}{1+\eta b}\right) \quad \text{with} \quad a = \frac{\Delta S_{z\, interface} + \frac{7}{2}<T_z>}{<S_z>_{bulk}} \quad \text{and} \quad b = \frac{\Delta L_z}{<L_z>_{bulk}} \qquad (15)$$

The results of Fig.5 suggest that the *a* and *b* coefficients are very similar. We can confirm this by calculating these values according to XMCD results in the case of Co:

$$a = \frac{\Delta S_{z\, interface} + \frac{7}{2}<T_z>}{<S_z>_{bulk}} \approx \frac{2-1.5}{1.5} = 0.33 \pm 0.06$$

$$\text{and} \quad b = \frac{\Delta L_z}{<L_z>_b} \approx \frac{0.21-0.16}{0.16} = 0.31 \pm 0.1 \qquad (16)$$

With this very simple analysis we finally show that the proportionality between $< S_z >_{eff}$ and $< L_z >$ results from a similar variation of ΔS_z and ΔL_z for Co at the Co/Ni interfaces. This analysis also shows that an increase of the true spin moment at the interface is highly possible. Indeed if we assume that the increase of the Co effective spin moment at the interface only comes from $< T_z >$,

this means that $< T_z > / < S_z > \approx 10\%$ which is quite unreasonable compared to our calculations or to literature [88]. According to *ab initio* calculations, $\Delta S_{z_{interface}}$ is around 3% and $\frac{7}{2}<T_z>$ around 9%. We observed a much larger effect but it is not possible to disentangle both variations in this study. Nevertheless, the possible increase of the spin moment at the interface is certainly not high since we do not detect it by using standard magnetometry measurements. Unfortunately, it is very difficult to apply this analysis to the Ni moments since the changes in the orbital moment relative to the error bars are small. Nevertheless, the calculations show that in Ni the $< T_z >$ contribution oscillates from positive to negative from one atomic layer to the other, leading to an average value close to zero. This explains why we do not see the same variation of the effective spin moment depending on the interface contribution as in Co. We thus do not observe a strong variation of the Ni moments which is in agreement with calculations. The fact that we observe a similar slope for Ni and Co in Fig.5 is simply fortuity. It just comes from the fact that this ratio is observed to be the same for the thick Co and Ni reference layers. Since Ni moments in the SLs are observed to only vary a little compared to the bulk, the spin to orbital moment ratio has to be almost constant as actually observed.

We can go further now by considering the physical process that may affect $< T_z >$. This operator describes the anisotropy of the electron spin-density distribution, which may be very sensitive to any chemical disorder at the interface since it strongly depends on the type of atoms surrounding the Co atom that absorbs the photon [94-96]. Any atomic exchange between Co and Ni at the interface thus may affect $< T_z >$. As our XMCD analysis clearly indicates similar variation of $< T_z >$ and $< L_z >$ for Co, this means that the anisotropy of the Co orbital moment at the interface also strongly depends on the chemical ordering at the interface. This conclusion is besides supported by the strong decrease of the PMA by growing an interface with 90% Co+10% Ni in contact with the Ni layer. We tried to get some information on the orbitals that are responsible for this increase of $< T_z >$ at the interface in order to identify some possible link between $< T_z >$ and $< L_z >$. Assuming that the magnetization is along the superlattice axis (Oz), $< T_z >$ is obtained for one of the Co or Ni atoms by summing the matrix elements of the operator $t_z=s_z\{1-3z^{^2}/r^{^2}\}$, for all electrons located inside the corresponding atomic sphere. The differences between the matrix elements of t_z calculated for all the non-equivalent atoms in their respective {d_{z^2}, d_{xz}, d_{yz}, $d_{x^2-y^2}$, d_{xy}} basis [99] should in particular be useful to understand why $< T_z >$ depends on the location of the atoms with respect to interfaces. Such qualitative analysis of $< T_z >$ in terms of atomic orbitals is however difficult, because the crystal-field and spin-orbit coupling contributions to $< T_z >$ must be both taken into account, and because the whole Brillouin zone must be considered. Further work is needed to reach this goal.

This work allows us finally to propose an explanation concerning the different PMA observed in (111) sputtered and MBE samples. On the one hand, the interface between two successively deposited materials using MBE can be very abrupt since the energy of the incoming atoms is thermic

and consequently small (around 0.1 eV). On the other hand, this energy is much larger during the sputtering process (at least several eV or more if a bias is used). This may lead to some atomic interchange at the interface even if the average interface may be very flat. Such a difference explains why we observed some lower contribution of $<T_z>$ in sputtered samples compared to the epitaxial ones. Since $<T_z>$ and $<L_z>$ are linked via the chemical ordering at the interface, this may explain why the observed PMA is lower in sputtered films than in epitaxial ones.

6 – Conclusion

In summary, we have studied in the detail the potential contributors to the PMA in Co/Ni layered structures. We find that "bulk" magnetoelastic effects cannot explain the magnitude of the PMA in Co/Ni(111) layers grown on Au or Cu. The magnetoelastic energy deduced from strain determination is actually shown to be much lower than the interface contribution. The origin of PMA in this system is thus attributed to the interface in addition to the bulk (111) magnetocrystalline anisotropy. While we attribute the interface anisotropy to the magnetocrystalline anisotropy (Neel interface anisotropy) the role of interfacial magnetoelastic contributions may also contribute. The XMCD analysis confirms the strong influence of the interfaces. Whereas the Ni moments are observed to be very similar to bulk values, strong enhancements of both the effective spin moments and orbital moments of Co are observed at the interface. Ab initio calculations allow us to show that the enhancement of the Co effective spin moment deduced from the spin sum rule is due to a strong contribution of the spin magnetic dipole operator at the interface for Co. The enhancement observed experimentally is however too strong to be assigned only to spin magnetic dipole operator, suggesting another contribution coming from the increase of the Co spin moment in contact with Ni. Moreover, the constant effective spin to orbital moment ratio observed in both MBE and sputtered samples suggests a clear dependence between the spin dipole operator and the orbital moment for Co atoms at the interfaces. The amplitude of this spin dipole operator for Co is observed to be lower in sputtered films compared to MBE layers, indicating some chemical disorder in the lattice at the Co/Ni interface compare to MBE. Finally, the interface anisotropy is observed to be clearly correlated to an increase of the perpendicular Co orbital moment at the interface with Ni. The lowest interfacial Co orbital moments observed in sputtered samples compared to MBE are consistent with a lowest spin dipole operator and interfacial spin moment contributions. This is explained by a lower interfacial chemical order in sputtered samples and we suggest that the PMA in Co/Ni samples should strongly vary with the growth process conditions, and especially to any Co and Ni atoms interchange mechanism at the interfaces.

REFERENCES

[1] David R. Lide,*CRC Handbook of Chemistry and Physics*, CRC Press LLC, 2004.

[2] J.C.A. Huang, T.E. Wang, C.C. Yu, Y.M. Hu, P.B. Lee, M.S. Yang, J.Cryst. growth171, 442 (1997)

[3] J. M. Gallego, S. Kim, T.J. Moran, D.Lederman, I. K. Schuller, Phys. Rev. B 51, 2550 (1995)

[4] G. H. O. Daalderop, P.J. Kelly, F. J. A. den Broeder, Phys. Rev. Lett. 68, 682 (1992)

[5] K.Kyuno, J.G. Ha, R. Yamamoto, S. Asano, Jpn. J. Appl. Phys. Vol. 35, 2774-2778 (1996)

[6] M. T. Johnson, J. J. de Vries, N. W. E. McGee, J. aandeStegge, F. J. A. den Broeder, Phys. Rev. Lett. 69, 3575 (1992)

[7] M.T. Johnson , F.J.A. den Broeder , J.J. de Vries , N.W.E. Mc Gee , R. Jungblut and J. aan de Stegge,J. Mag. Mag. Mat. 121, 494(1993)

[8] Y. B. Zhang,J. A. Woollam, Z. S. Shan, J. X. Shen, D. J. Sellmyer, IEEE Trans. Mag. 30, NO. 6. (1994)

[9] J.-M.L. Beaujour, W. Chen, K. Krycka, C.-C.Kao,J. Z. Sun, A. D. Kent, Eur. Phys. J. B 59, 475(2007)

[10] S. Girod, M. Gottwald, S. Andrieu, S. Mangin, J. Mc Cord, E. E. Fullerton, J.-M.L. Beaujour, B.J. Krishnatreya, A.D.Kent, Appl. Phys. Lett. 94, 262504 (2009)

[11] M. Gottwald, S. Girod, S. Andrieu, S. Mangin, IOP Conf.Series: Materials Science and Engineering 12 (2010) 012018

[12] F.J.A. den Broeder, E. Janssen, W. Hoving and W.B.Zeper, IEEE Trans. Mag., VOL.28, NO. 5, p. 2760, (1992)

[13] Y. B. Zhang, P. He, J. A. Woollam, J. X. Shen, R. D. Kirby, D. J. Sellmyer, J. Appl. Phys. 75, 6495 (1994)

[14] V. M. Naik, S. Hameed, R. Naik, L. Pust, L. E. Wenger, G. L. Dunifer, G. W. Auner, J. Appl. Phys. 84, 3273 (1998)

[15] H.Kurt, M. Venkatesan,J.M.D. Coey, J. Appl. Phys108, 073916 (2010)

[16] Y. B. Zhang and J. A. Woollam, IEEE Trans. Mag., vol. 31, NO. 6, p. 3262 (1995)

   O. Posth, C. Hassel, M. Spasova, G. Dumpich and J. Lindner, S. Mangin, J. Appl Phys **106** 023919 (2009)

[17] D. Stanescu, D. Ravelosona, V. Mathet, C. Chappert, Y. Samson, C. Beigné, N. Vernier, J. Ferré, J. Gierak, E. Bouhris, and E.E. Fullerton, J. Appl. Phys. 103,07B529 (2008)

[18] J. M. Gallego, D. Lederman, T. J. Moran, Ivan K. Schuller, Appl. Phys. Lett. **64**, 2590 (1994)

[19] C. Prados, D. Garcia, F. Lesmes, J.J. Freijo, A. Hernando, Appl. Phys. Lett. 67, 718 (1995)

[20] D. Han, Appl. Phys. Lett. 68, 2-15-2154 (1996)

[21] D.H. Han, IEEE Trans. Mag. 32, 4585(1996)

[22] J.M. Freitag, J.O. Strom-Olsen, Z.Altounian, R.W. Cochrane, Mat. Res. Soc. Symp. Proc. Vol. 475, P.475 (1997)

[23] R.J. Pollard, S.E. McCartney, R. Atkinson,J. Mag. Mag. Mat. 176, 134 (1997)

[24] R.J. Pollard, S.E. McCartney and R. Atkinson, IEEE Trans. Mag. Vol. 34, No. 4, p. 879 (1998)

[25] F. Lesmes, A. Salcedo, J.J. Freijo, D. Garcia, A. Hernando, C. Prados, Appl. Phys. Lett. 69, (1996)

[26] J.M. Gallego, D. Lederman, S. Kim, and I. K. Schuller, Phys. Rev. Lett.74, 4515 (1995)

[27] S. Kim, D. Lederman, J.M.Gallego, I. K. Schuller, Phys. Rev. B 54, 5291 (1996)

[28] J.M. Gallego, S. Kim, D. Lederman, and I. K. Schuller, J. Mag. Mag. Mat.156 (1996) 397-398

[29] M. Weissmann, A. M.Llois, R. Ramirez, M. Kiwi, Phys. Rev. B 54, 15335 (1996)

[30] B.Y. Yavorsky, I. Mertig , V.N. Antonov, Phase Transitions, Vol.76, 481 (2003)

[31] L.Chico, M.P. Lopez-Sancho, M.C. Munoz, Phys. Rev. B 65, 184429 (2002)

[32] C. Hartmann, C. Mathieu, B. Hillebrands, S. Kim, I. K. Schuller, Phys. Rev. B 55, 14074 (1997)

[33] L. Berger, Phys. Rev. B 54, 9353 (1996)

[34] J.C. Slonczewski, J. Magn. Magn.Mater.159, L1 (1996).

[35] M. Tsoi, A.G.M. Jansen, J. Bass, W.-C. Chiang, M. Seck, V. Tsoi, P. Wyder, Phys. Rev. Lett. 80, 4281 (1998)

[36] J.A. Katine, F.J.Albert, R.A.Buhrman, E.B. Myers,D.C.Ralph, Phys. Rev. Lett. 84, 3149 (2000)

[37] S. Mangin, D. Ravelosona, J.A. Katine, M.J. Carey, B.D. Terris, E E. Fullerton, Nat. Mat. 5, 210 (2006)

[38] D. Ravelosona, S.Mangin, J.A.Katine, E.E. Fullerton, B.D. Terris, Appl. Phys. Lett. 90,072508 (2007)

[39] Luqiao Liu, Takahiro Moriyama, D.C. Ralph,R.A.Buhrman, Appl. Phys.Lett. 94, 122508 (2009)

[40] S.Mangin, Y. Henry,D. Ravelosona, J.A. Katine, E.E. Fullerton, Appl. Phys.Lett. 94, 012502 (2009)

[41] D. Ravelosona, S. Mangin, Y. Lemaho, J. A. Katine, B. D. Terris, and Eric E. Fullerton, Phys. Rev. Lett. 96, 186604 (2006)

[42] J. Cucchiara, Y. Henry, D. Ravelosona, D. Lacour, E.E. Fullerton, J.A. Katine, S. Mangin, Appl. Phys.Lett. 94,102503 (2009)

[43] W. H. Rippard, A. M. Deac, M. R. Pufall, J. M. Shaw, M. W. Keller, S. E. Russek, G. E. W. Bauer, C. Serpico, Phys. Rev. B 81, 014426 (2010)

[44] M. W. Keller, M.R. Pufall, W.H. Rippard, and T.J. Silva, Phys. Rev. B 82, 054416 (2010)

[45] D. Bedau, H. Liu, J. Z. Sun, J. A. Katine, E. E. Fullerton, S. Mangin, A. D. Kent, Appl. Phys. Lett. 97, 262502 (2010)

[46] D. Bedau, H. Liu, J.-J. Bouzaglou, A. D. Kent, J. Z. Sun, J. A. Katine, E. E. Fullerton, and S. Mangin, Appl. Phys. Lett. 96, 022514 (2010)

[47] N. Reckers, J. Cucchiara, O. Posth, C. Hassel, F. M. Römer, R. Narkowicz, R. A. Gallardo, P. Landeros, H. Zähres, S. Mangin, J. A. Katine, E. E. Fullerton, G. Dumpich, R. Meckenstock, J. Lindner, and M. Farle, Phys. Rev. B 83, 184427 (2011)

[48] Weiwei Lin (林维维), J. Cucchiara, C. Berthelot, T. Hauet, Y. Henry, J. A. Katine, E. E. Fullerton, and S. Mangin, Appl. Phys. Lett. 96, 252503 (2010)

[49] Y. Henry, S. Mangin, J. Cucchiara, J. A. Katine, E. E. Fullerton, Phys. Rev. B 79, 214422 (2009)

[50] D.B. Gopman, D. Bedau, S. Mangin, C.H. Lambert, E.E. Fullerton, J.A. Katine, and A.D. Kent, Appl. Phys. Lett. 100, 062404 (2012)

[51] J.-M.L. Beaujour, W. Chen, K. Krycka, C.-C.Kao,J. Z. Sun, A. D. Kent., Eur. Phys. J. B 59, 475 (2007)

[52] W.Chen, J.-M.L. Beaujour, G. deLoubens, A.D. Kent, Appl. Phys. Lett. 92,012507 (2008)

[53] S. Mizukami, X. Zhang, T. Kubota, H. Naganuma, M. Oogane , Y. Ando, T. Miyazaki, Applied Physics Express 4, 013005 (2011)

[54] J.-M.Beaujour, D.Ravelosona, I.Tudosa,E.E.Fullerton, A.D. Kent, Phys. Rev. B 80, 180415(R) (2009)

[55] T. Kato , Y. Matsumoto , S. Okamoto , N. Kikuchi , O. Kitakami, N. Nishizawa, S. Tsunashima, S. Iwata, IEEE Trans. Mag. 47, NO.10, p. 3036 (2011)

[56] J. M. Shaw, H. T. Nembach, and T.J.Silva, Appl. Phys. Lett. 99,012503 (2011)

[57] Zhenya Li, Zongzhi Zhang, Hui Zhao, Bin Ma, and Q.Y.Jin, J. Appl. Phys. 106, 013907 (2009)

[58] H.Y.T. Nguyen, R. Acharyya, E. Huey, B. Richard, R. Loloee, W.P. Pratt, Jr.,and J.Bass, Shuai Wang and Ke Xia, Phys. Rev. B 82, 220401(R) (2010)

[59] F. Gimbert, L. Calmels and S. Andrieu, Phys. Rev. B 84, 094432 (2011)

[60]C. Burrowes, D. Ravelosona, C. Chappert, S. Mangin, E.E. Fullerton, J.A. Katine, B.D. Terris, Appl. Phys. Lett. 93, 172513 (2008)

[61] C. Burrowes ,A.P.Mihai , D.Ravelosona, J.-V.Kim, C.Chappert , L.Vila , A. Marty, Y.Samson, F.Garcia-Sanchez , L.D.Buda-Prejbeanu, I. Tudosa, E.E.Fullerton and J.-P. Attané, Nat. Phys. 6, 17 (2010)

[62] T.Koyama, D.Chiba , K.Ueda, K.Kondou , H.Tanigawa , S.Fukami , T.Suzuki , N.Ohshima, N. Ishiwata, Y. Nakatani , K. Kobayashi and T. Ono, Nat. Mat. 10, 194 (2011)

[63] S. Fukami, T. Suzuki, K. Nagahara, N. Ohshima, Y. Ozaki, S. Saito, R. Nebashi, N. Sakimura, H. Honjo, K. Mori, C. Igarashi, S. Miura, N. Ishiwata, and T. Sugibayashi, 2009 Symposium on VLSI Technology Digest of Technical Papers

[64] T. Suzuki, S. Fukami, K. Nagahara, N. Ohshima, and N. Ishiwata, IEEE Trans. Mag. 45, NO.10, p. 3776 (2009)

[65] T. Moriyama, T. J. Gudmundsen, P. Y. Huang, L. Liu, D. A. Muller, D. C. Ralph , and R. A. Buhrman, Appl. Phys. Lett. 97, 072513 (2010)

[66] Z.R. Tadisina, A. Natarajarathinam, and S. Gupta, J. Vac. Sci. Technol. A28, 973 (2010)

[67] O. Hellwig, T. Hauet, T. Thomson, E.Dobisz, J.D. Risner-Jamtgaard, D.Yaney, B.D.Terris, E.E. Fullerton, Appl. Phys. Lett. 95, 232505 (2009)

[68] T. Hauet, E. Dobisz, S. Florez, J. Park, B. Lengsfield, B.D. Terris, and O. Hellwig, Appl. Phys. Lett. 95,262504 (2009)

[69] S. S. Dhesi, E. Dudzik, H. A. Dürr, G. van der Laan, N. B. Brookes, J. Appl. Phys. 87, 5466 (2000)

[70] S. S. Dhesi, H. A. Dürr, E. Dudzik, G. van der Laan, N. B. Brookes, Phys. Rev. B 61, 6866 (2000)

[71] C.A.F. Vaz, G. Lauhoff , J.A.C. Blanda, S. Langridge , D.G.Bucknall ,J.Penfoldb , J.Clarke ,S.K.Halder , B.K.Tanner, J. Mag. Mag. Mat. 313, 89 (2007)

[72] F. Gimbert, L. Calmels, J. Appl. Phys. 109(07C109):1–3, (2011)

[73] *Science of Microscopy*, Vol. 1, Part I, Ch. 2. (Eds. P. W. Hawkes, J. C. H. Spence), Springer Science + Business Media, LLC, New York, USA (2006)

[74] M. J. Hytch, E. Snoeck and R. Kilaas, Ultramicroscopy 74, 131-146 (1998).

[75] D. Sander, J. Phys. Condens. Matter 16, R603 (2004)

[76] S. Andrieu, F. Lahatra Razafindramisa, E. Snoeck, H. Renevier, A. Barbara, J.M. Tonnerre, M. Brunel, M.Piecuch, Phys. Rev. B, 52, (1995), p.9938-9951

[77] L.D. Landau, E.M. Lifshitz, *Theory of elasticity*, 3rd edition by Butterworth-Heinemann, (1986)

[78] Kai Yanga, Takayoshi Anan, Leo J. Schowalter, Appl. Phys. Lett. 65, 2789 (1994)

[79] E.A.M. van Alphen, S.G.E te Velthuis, H.A.M. de Gronckel, K. Kopinga, W.J.M. de Jonge, Phys. Rev. B 49, 17336 (1994)

[80] G. Bochi, C.A. Ballentine, H.E. Inglefield, C.V. Thompson, R.C. O'Handley, J. Appl. Phys. 79, 5845 (1996)

[81] R. Nakajima, J. Stöhr, and Y. U. Idzerda, Phys. Rev. B 59, 6421 (1999)

[82] M. Sicot, S. Andrieu, P. Turban, Y. Fagot-Révurat, H. Cercellier, A. Tagliaferri, C. De Nadai, N.B. Brookes, F. Bertran, F.Fortuna, Phys. Rev. B, 68, 184406 (2003)

[83] J. Stöhr H.C. Siegmann, *Magnetism : from fundamental to nanoscale dynamics*, Springer series in solid state science, ed. Springer Verlag, (2006) ISSN : 0171-1873

[84] B.T. Thole, P. Carra, F. Sette, G. van der Laan, Phys. Rev. Lett. 68, (1992), 1943.

[85] P. Carra, B.T. Thole, M. Altarelli, X. Wang, Phys. Rev. Lett. 70, (1993), 694.

[86] C. T. Chen et al., Phys. Rev. Lett. 75, 152 (1995)

[87] T. Oguchi, T. Shishidou, Phys. Rev. B 70, 024412 (2004)

[88] R. Wu and A. J. Freeman, Phys. Rev. Lett. 73, 1994 (1994)

[89] P. Blaha, K. Schwarz, G. K. H. Madsen, D. Kvasnicka, and J. Luits, Wien2k, *An Augmented Plane Wave+Local Orbitals Program for Calculating Crystal Properties* (K. Schwarz, Vienna, Austria, 2001)

[90] O. Eriksson, B. Johansson, R. C. Albers, A. M. Boring, and M. S. S. Brooks, Phys. Rev. B **42**, 2707 (1990)

[91] M. S. Brooks, Physica B **130**, 6 (1985)

[92] R. Robles, A. Bergman, A. B. Klautau, O. Eriksson, and L. Nordström, J. Phys. Condens. Matter **20**, 015001 (2008)

[93] C. O. Rodriguez, M. V. Ganduglia-Pirovano, E. L. Peltzer y Blancá, M. Petersen, and P. Novák, Phys. Rev. B **63**, 184413 (2001)

[94] C. Ederer, M. Komelj, M. Fähnle, and G. Schütz, Phys. Rev. B **66**, 094413 (2002)

[95] M. Komelj,C. Ederer, J. W. Davenport, and M. Fähnle, Phys. Rev. B **66**, 140407 (2002)

[96] C. Ederer, M. Komelj, and M. Fähnle, Phys. Rev. B 68, 052402 (2003)

[97] D. Weller, J. Stöhr, R. Nakajima, A. Carl, M.G. Samant, C. Chappert, R. Mégy, P. Beauvillain, P. Veillet, G.A. Held, Phys. Rev. Lett. 75, 3752 (1995)

[98] P. Söderlind, O. Eriksson, B. Johansson, R. C. Albers, and A. M. Boring, Phys. Rev. B **45**, 12911 (1992)

[99] J. P. Crocombette, B. T. Thole, and F. Jollet, J. Phys.: Condens. Matter 8, 4095 (1996)

TABLES

	$a_{//}(100)$ (nm)	$\varepsilon_{//}^{Ni}$ (%)	$\varepsilon_{\perp}^{Ni}$ (%)	$\varepsilon_{//}^{Co}$ (%)	$\varepsilon_{\perp}^{Co}$ (%)	$d_{\perp}^{Ni}(111)$ (nm)	$d_{\perp}^{Co}(111)$ (nm)	$<d>(111)$ (nm)
Measured	0.3537							0.2040
Calculated (isotropic)	0.35363	+0.36	-0.41	-0.24	+0.33	0.20260	0.20535	0.20397
Calculated (general)	0.35330	+0.27	-0.21	-0.33	+0.17	0.20302	0.20502	0.20404

TABLE 1 : lattice distances measured by XRD on a (Co$_{3ML}$Ni$_{3ML}$)x75 superlattice (fig.2) compared to calculation using elastic theory. The calculation were performed assuming first a perfect isotropic crystal (that is C$_{11}$-C$_{12}$=C$_{44}$) and with a more realistic approach including the anisotropic elastic behavior (from [78]). In both cases the agreement is very good.

	bulk *hcp* Co	bulk *fcc* Ni
atomic sphere	1.64	0.63
atomic sphere + interstitial area	1.60	0.61
experiments	1.5 [98]; 1.55 [86] 1.5±0.1 (this work)	0.5 [98] 0.52±0.05 (this work)

TABLE 2. Spin magnetic moment (in Bohr magneton μ$_B$) calculated with the code Wien2k for Co in bulk *hcp* Co and for Ni in bulk *fcc* Ni. Values measured experimentally are given for comparison.

	bulk *hcp* Co	bulk *fcc* Ni
without OP	0.083	0.051
with OP	0,13	0.069
experiments	0.14 [98] 0.16±0.02 (this work)	0.05 [98] 0.056±0.005 (this work)

TABLE 3. Orbital magnetic moment (in Bohr magneton μ$_B$) calculated with the code Wien2k for Co in bulk *hcp* Co and for Ni in bulk *fcc* Ni, with or without orbital polarization (OP) correction. Values measured experimentally are given for comparison.

Ni	Ni	Ni	Co	Co	Co	Co	Co	<Ni>	<Co>
0.646	0.568	0.646	1.701					0.620	1.701
0.638	0.583	0.638	1.658	1.658				0.620	1.658
0.649	0.587	0.649	1.683	1.650	1.683			0.628	1.672
0.638	0.581	0.638	1.667	1.644	1.644	1.667		0.619	1.656
0.642	0.582	0.642	1.678	1.647	1.658	1.647	1.678	0.622	1.662

TABLE 4. Spin magnetic moment (in Bohr magneton μ_B) calculated with the code Wien2k for Co and Ni atoms in the monolayers of the Co_{xML}/Ni_{3ML} superlattice period. The averaged value of the Co and Ni spin magnetic moments are also given.

Ni	Ni	Ni	Co	Co	Co	Co	Co	<Ni>	<Co>
0.00826	-0.01104	0.00826	0.01967					0.00183	0.01967
0.00441	-0.00814	0.00441	0.00846	0.00846				0.00023	0.00846
0.00529	-0.00866	0.00529	0.00995	0.00062	0.00995			0.00064	0.00684
0.00516	-0.00793	0.00516	0.00726	0.00000	0.00000	0.00726		0.00080	0.00363
0.00664	-0.00786	0.00664	0.00935	-0.00026	0.00219	-0.00026	0.00935	0.00181	0.00407

TABLE 5. Value of the magnetic dipole operator T_z (in $\hbar$) calculated with the code Wien2k for Co and Ni atoms in the monolayers of the Co_{xML}/Ni_{3ML} superlattice period. The values averaged over all the Co and Ni atoms of the superlattices are also given. It should be noted that T_z is oscillating in Ni layers, leading to a T_z average close to zero, contrary to Co where T_z is strongly attenuated between the interfaces (see inset in fig.10).

Ni	Ni	Ni	Co	Co	Co	Co	Co	<Ni>	<Co>
0.066	0.063	0.066	0.123					0.065	0.123
0.060	0.064	0.060	0.125	0.125				0.061	0.125
0.062	0.066	0.062	0.126	0.123	0.126			0.063	0.125
0.063	0.067	0.063	0.130	0.121	0.121	0.130		0.064	0.126
0.062	0.066	0.062	0.129	0.124	0.116	0.124	0.129	0.063	0.124

TABLE 6. Orbital magnetic moment (in Bohr magneton μ_B) calculated with the code Wien2k for Co and Ni atoms in the monolayers of the Co_{xML}/Ni_{3ML} superlattice period. The averaged value of the Co and Ni orbital magnetic moments are also given. The orbital polarization correction is taken into account.

Figure captions

FIGURE 1: STEM analysis of a $(Co_{1ML}Ni_{3ML})x20$ / Au $(Co_{3ML}Ni_{3ML})x20$ spin valve : *-top-* Low magnification HAADF image showing the Au and Co/Ni stacking and, adjusting the contrast, the Co/Ni bilayers inset. *-Bottom left-* Atomic resolution HAADF image of the Co/Ni layer evidencing the FCC structure of the stacking. *-Bottom right-* GPA measurement of the relative out-of plane deformation of the Co/Ni and Au (111) planes showing the fully relaxation of the two stackings.

FIGURE 2 : Structure analysis of an Al_2O_3/V/Au/ $(Co_{3ML}Ni_{3ML})x75$ / Au superlattice : *-left-* X-Ray diffraction θ-2θ spectrum which gives d(111)= 0.2040nm. *-right-* in-plane X-Ray diffraction spectrum which gives d(110)= 0.2501nm (X-Ray wavelength Cu Kα).

FIGURE 3 : (a) architecture of the wedges and (b) intensity at the L_3 Co edge for two wedges with a Co thickness variation in the range 0.25 to 10 monolayers. Each region of constant Co thickness is around 3mm long. (c) Isotropic absorption curves measured on the wedges and (d) corresponding variation of the *L3* edge for both Co and Ni. The Ni and Co edges are more attenuated by the capping for wedge 1 due to a slightly thicker capping. (e) After correction, the Co edge follows an exponential increase which allows us to precisely determine the escape depth λ. (f) Using the equation in the text, the Co to Ni intensity ratio is perfectly reproduced.

FIGURE 4 : For each Co thickness of the two wedges, hysteresis loops at the Co L_3 edge are performed with the field applied along the normal of the samples. The magnetization is clearly perpendicular to the film plane for Co thickness up to 4ML, and turns in plane above 4ML.

FIGURE 5 : (left) Co and Ni absorption edges performed on a $(Co_{1ML}/Ni_{3ML})x5$ superlattice measured by applying both right and left light polarization and ± 0.5T applied magnetic field – see text-, and corresponding XMCD signal with XMCD signal integration. All this curves are obtained without any absorption baseline correction which allows a precise determination of Co and Ni orbital to effective spin magnetic moments ratio calculated using *p* and *q*. (right)

variation of the effective spin moment with the orbital magnetic moment in MBE and sputtered samples for both Co and Ni edges

FIGURE 6 : plot of the effective spin and orbital magnetic moments for Co versus the Co thickness t_{Co} (left) and the inverse of t_{Co} (right) for a series of superlattices and for the wedges of figure 1. The two regimes described by gray lines are due to the existence of two different Co magnetic contributions, one at the interface with Ni, the other for Co surrounded by Co. The bulk values are obtained on a thick hcp Co film grown by MBE.

FIGURE 7 : plot of the effective spin and orbital magnetic moments for Ni in a series of Co/Ni superlattices : -*left*- for a fixed Ni thickness equal o 3ML and varying the Co thickness, -*right*- for a fixed Co thickness equal to 1ML and varying the Ni thickness. The bulk values are obtained on a thick fcc Ni film grown by MBE.

FIGURE 8 : plot of the effective spin and orbital magnetic moments of Co (left) and Ni (right) versus the Co thickness t_{Co} for the sputtered samples. The indicated bulk values are those obtained on thick Co and Ni MBE samples.

FIGURE 9 : Averaged values of $< M_{spin} >$ and $< M_{spin} >_{eff}$ calculated for a cobalt atom in Co_{xML}/Ni_{3ML} superlattices, as a function of the Co layer thickness.

FIGURE 10 : Calculated value of the z-component of the spin magnetic dipole operator, averaged over the Co and Ni atoms of Co_{xML}/Ni_{3ML} superlattices. The results are given as a function of the Co layer thickness. The inset described the spatial variations of $< T_z >$ in a period of the Co_{5ML}/Ni_{3ML} superlattice.
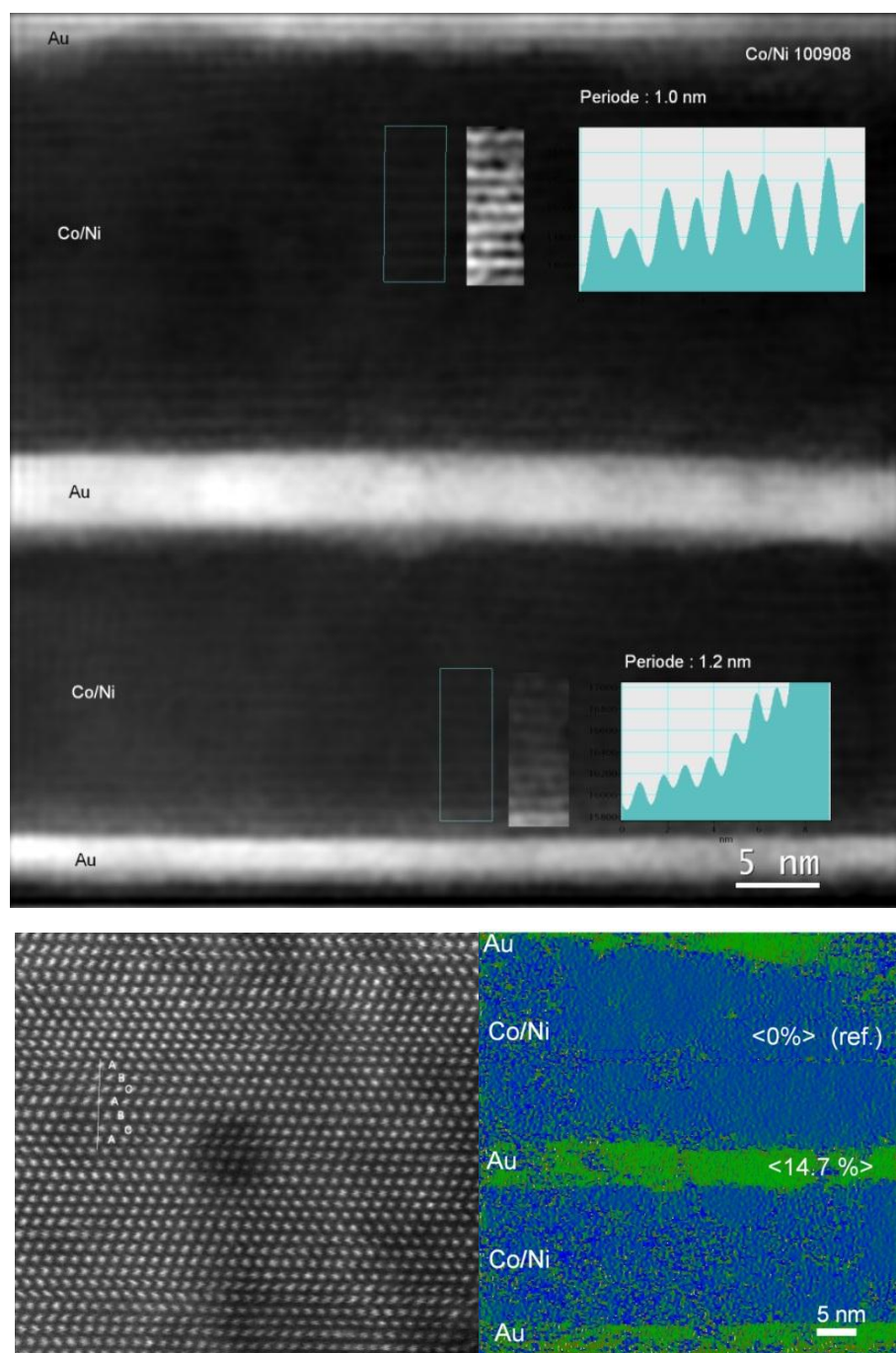
Figure 1

Figure 2
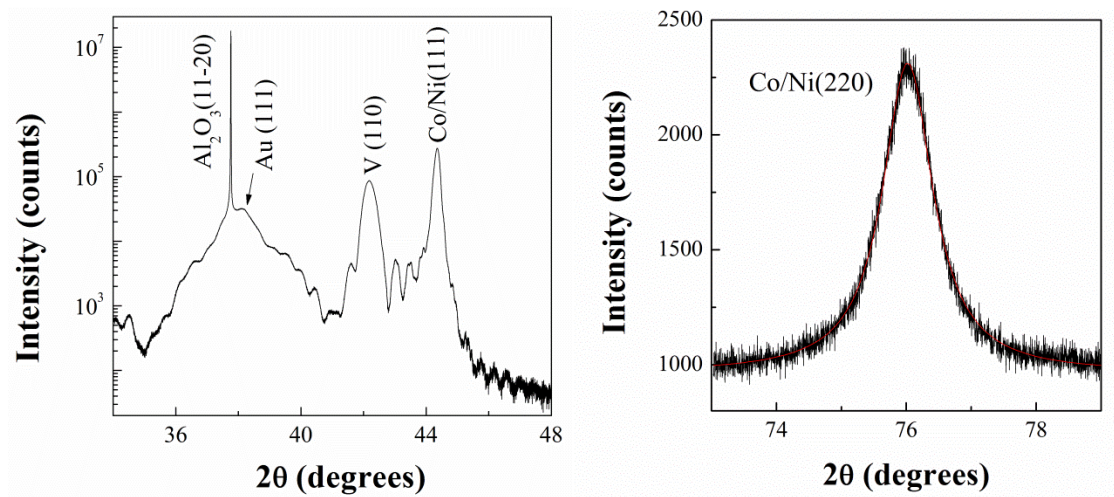
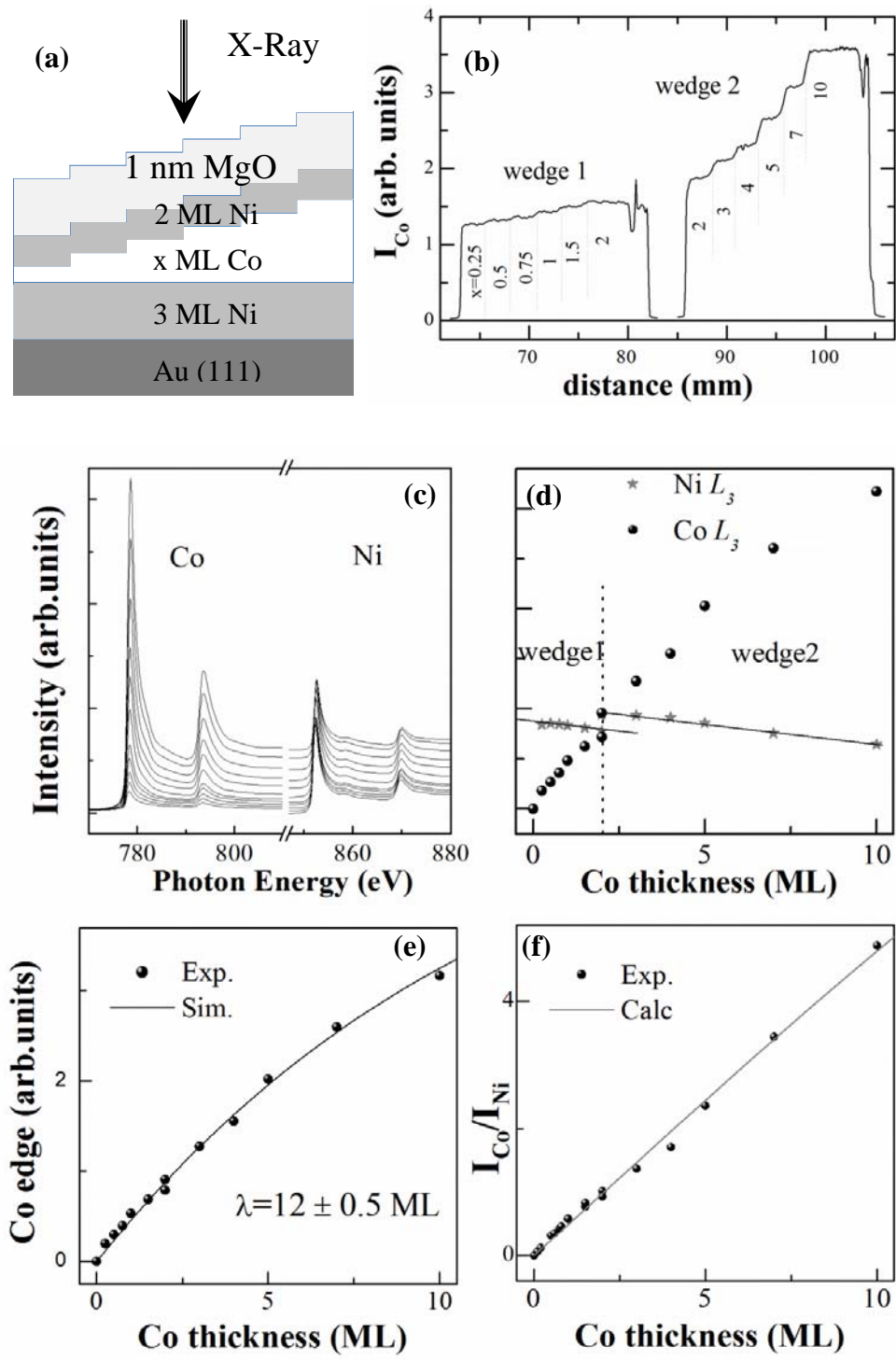*Figure 3*
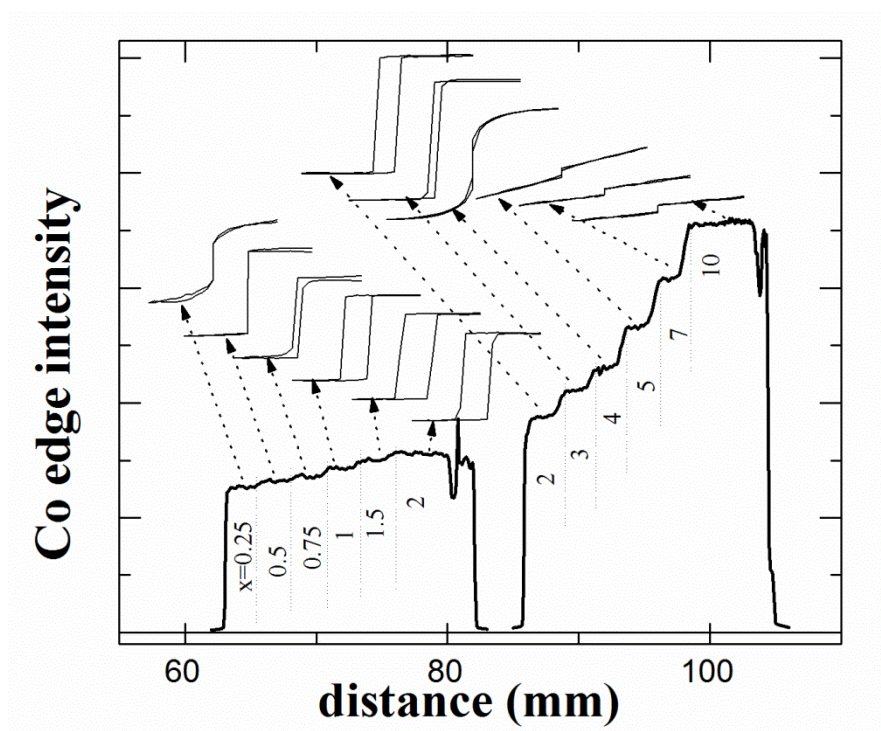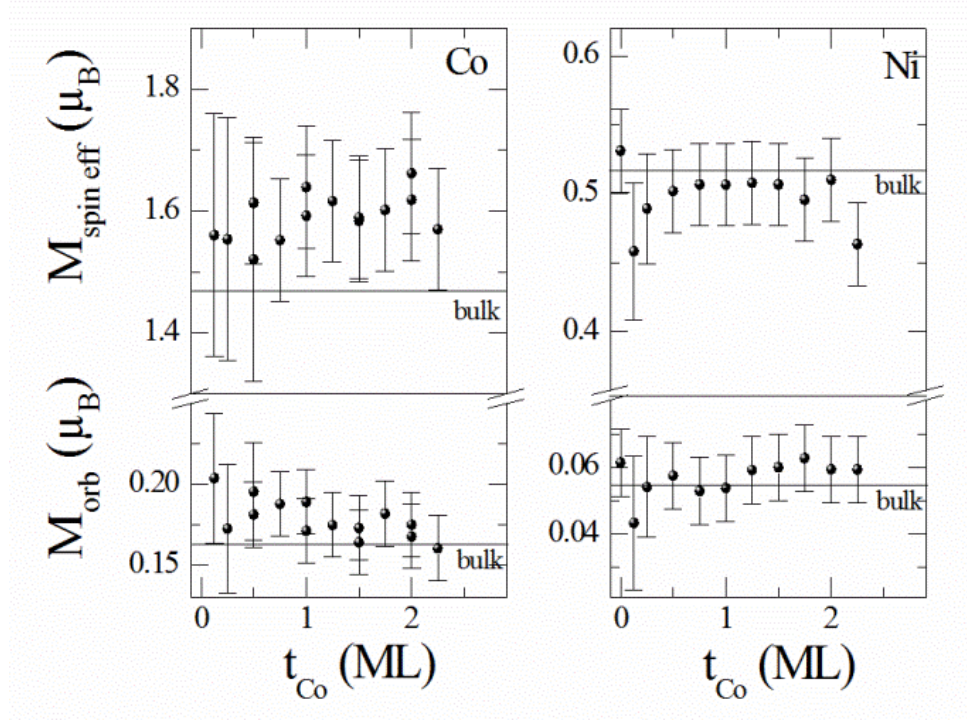
Figure 4
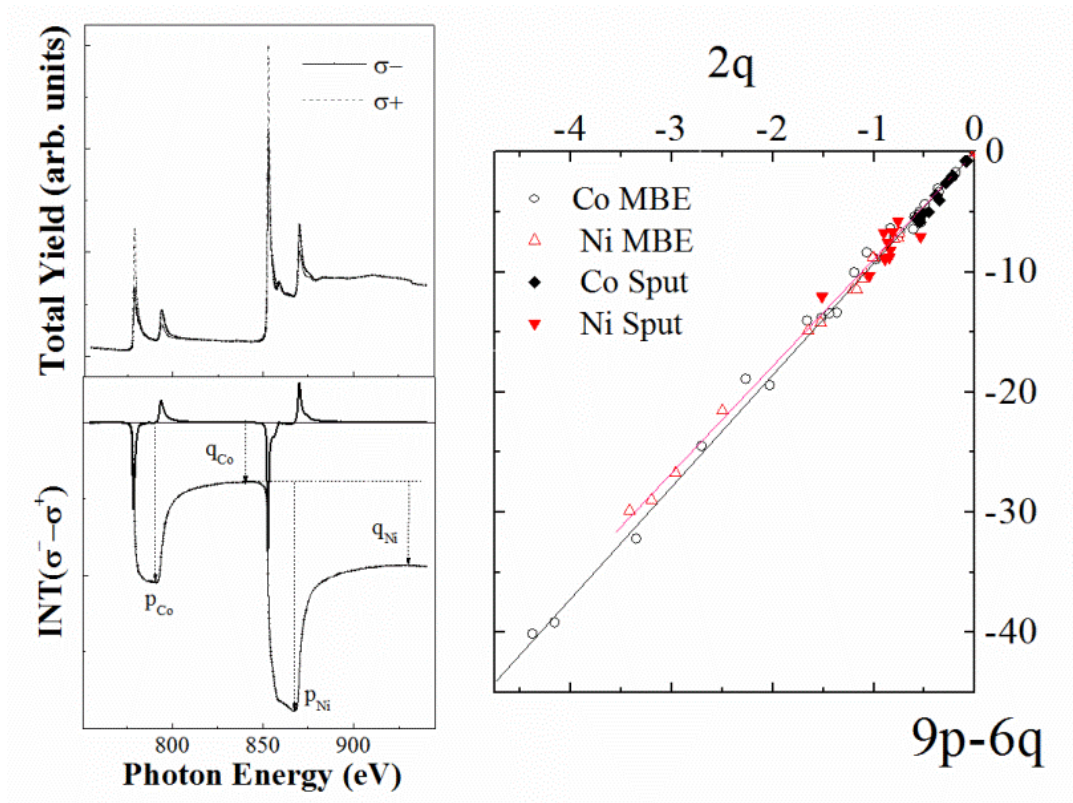
Figure 5
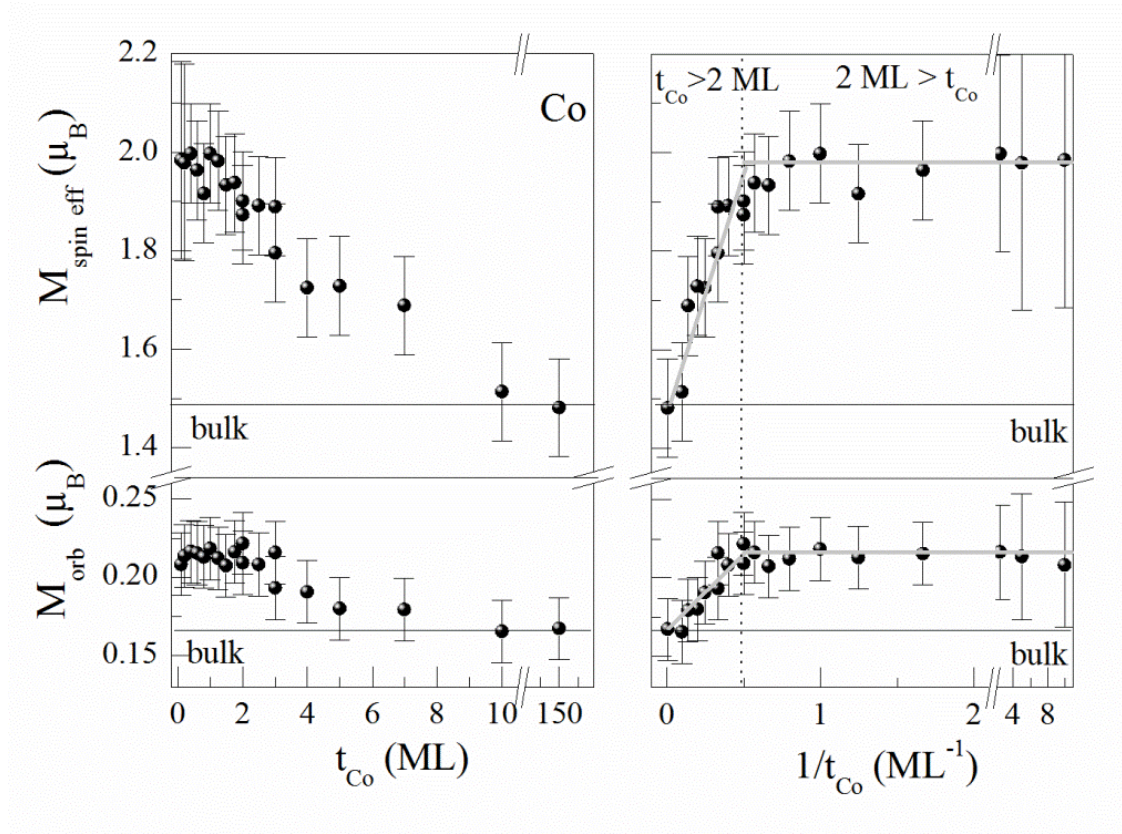
Figure 6
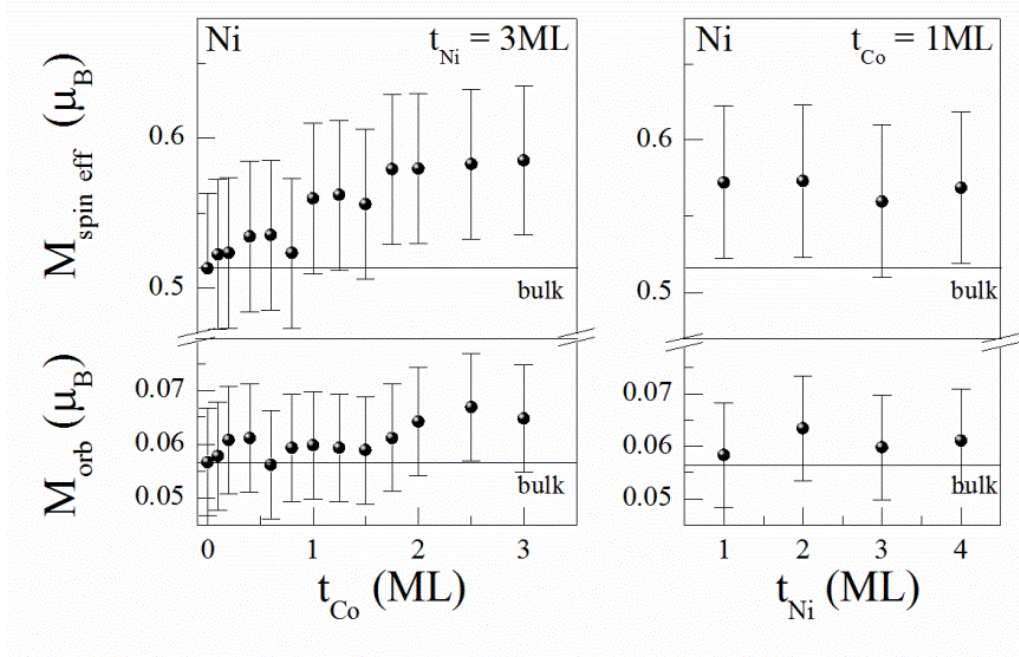
Figure 7

Figure 8

Figure 9

Figure 10